Biomass Conversion and Biorefinery (2024) 14:15283–15296
https://doi.org/10.1007/s13399-022-03697-2

ORIGINAL ARTICLE

Green synthesis of Au/ZnO nanoparticles for anticancer activity and oxidative stress against MCF-7 cell lines

Qasim R. Shochah[1] · **Ferdous A. Jabir**[2]

Received: 20 September 2022 / Revised: 15 December 2022 / Accepted: 20 December 2022 / Published online: 6 January 2023

Abstract

Cancer still kills more lives and causes heavy losses to countries' economies, despite the advance in its diagnosis and treatment methods. Nanotechnology has opened new and promising horizons in exploiting the distinct properties of nanomaterials. This study aimed to examine the activity of decorating gold (Au) on zinc oxide (ZnO) in treating breast cancer cells (MCF-7). In this work, we used *Hibiscus sabdariffa* flower extract in green synthesis ZnO, Au, and Au/ZnO nanoparticles (NPs) and characterized by UV–Vis, FTIR, XRD, FESEM, EDX, TEM, and BET techniques. ZnO, Au, and Au/ZnO NPs were evaluated for viability in MCF-7 cells, and oxidative stress was tested by determining the activity of antioxidant enzymes, lipid peroxidation, and calcium ions levels. The results indicated that the synthesized NPs had spherical or semi-spherical irregular shapes with an average size of 50.7, 51.6, and 8.45 nm for ZnO, Au/ZnO, and Au NPs, respectively. The inhibitory concentration (IC_{50}) was calculated to be 33.5, 28.7, and 34.9 µg/mL for ZnO, Au, and Au/ZnO NPs, respectively. The findings of this study show that the synthesized NPs caused a reduction in the antioxidant enzyme activity and increased levels of lipids peroxidation and calcium ions in the exposed cells compared to the untreated cells. The results of the measurements indicate that the Au/ZnO NPs were less cytotoxic against MCf-7 cells in vitro than the ZnO NPs at concentrations up to 30 µg/mL and alteration oxidation stress.

Keywords A green synthesis · Au/ZnO NPs · Cytotoxicity · MCF-7 · Lipid peroxidation · Enzymes antioxidant

1 Introduction

Cancer involves a huge group that includes more than 100 diseases. All cancers start because of abnormal and uncontrolled cell growth. Cancer is a disease that can affect any body organ and is considered the primary cause of death worldwide [1]. Traditionally, cancer therapeutic strategies are classified according to the treatment used, such as surgery, radiation, chemotherapy, targeted therapy, and immunotherapy. Chemotherapy alone, and in conjunction with other types of treatment, is used to treat localized and metastatic malignancies. Troubles such as solubility selectivity and degree of resistance are determinants of anticancer use to overcome these issues, particularly drug resistance. Much research was done, the most notable of which was the usage of nanotechnology [2]. Furthermore, nanotechnology has opened up new avenues for creating more effective treatment methods. Nanoparticles' potential medicinal advantages were initially proposed in the 1970s [3]. Compared to traditional drug administration, nano medicines preferentially accumulate in the tumor region because of the tumor's increased permeability and retention (EPR).

Metal oxide NPs have received significant interest from researchers due to their wide variety of applications in biology, medicine, and electronics. ZnO is a material that is frequently utilized in many areas of nanotechnology. These areas include biomedicine, the ceramics industry, photocatalytic applications, and an antibacterial agent [4].

Gold nanoparticles have received great attention due to their unique characteristics in drug administration, sensing, imaging, and chemotherapy. The biocompatibility of gold nanoparticles is an excellent feature of its advantageous features, in addition to simple synthesis and simple size control. They also offer high stability in most in vivo circumstances, tunable surface properties, and dense loading capabilities,

✉ Ferdous A. Jabir
ferdous.alturaihy@qu.edu.iq

[1] Department of Chemistry, College of Education, University of Al-Qadisiyah, Al-Diwaniya, Iraq

[2] Department of Medical Chemistry, College of Medicine, University of Al-Qadisiyah, Al-Diwaniya, Iraq

allowing precise cell targeting [5]. Gold nanoparticles have been used successfully as versatile, selective, and highly multifunctional antitumor therapeutics. Their surfaces may be functionalized with diverse biological molecules, inducing specialized functionalities, target selectivity, and stability in natural settings [6]. Among various hybrid metal NPs, metal /ZnO NPs with their excellent characteristics such as anti-inflammatory, biocompatibility, easy synthesis, and enhanced cytotoxicity are exhibiting significant application and efficiency as anticancer agents due to their highly selective properties and forcefulness against cancer cells [7–9].

Hybrid metal–semiconductor nanoparticles such as Au/ZnO, Ag/ZnO, and Mg/ZnO [10] have attracted significant attention from both the fundamental essential scientific and technological points of view. These nanocomposite materials not only combine the unique properties of the metal and the semiconductor but can also generate new properties due to the metal–semiconductor interface in the nanocomposite structure [11]. Nanoparticles can be formed utilizing various physical, chemical, and biological approaches [12]. Because they emit toxic by-products that are potentially ecologically damaging, the fabrication of nanoparticles utilizing physical and chemical approaches transfers the risk of toxicity and environmental contamination. According to preceding literature studies, ZnO NPs have been produced from numerous plant extracts like *Ficus religiosa* and *Azadirachta indica* [13], *Pontederia crassipes* [14], and *Pandanus odorifer* leaf [15].

Reactive oxygen species (ROS) levels rise to levels that outweigh the antioxidant defense mechanisms, causing oxidative stress to develop in the cell. An increase in reactive oxygen and nitrogen species (RONS) results from the physiological process of cellular oxidation. While oxygen is necessary for life in healthy conditions, it is also hazardous because it causes the development of free radicals, which are harmful to the body [16]. Groups of antioxidant enzymes, such as superoxide dismutases (SOD), catalase (CAT), and glutathione peroxidase (GPx), as well as non-enzymatic antioxidants such as glutathione (GSH), are involved in the cellular defense mechanism in living cells. Because these enzymes operate as biomarkers to discover oxidative damage to biomolecules and DNA, they can protect membranes, lipids, and proteins against oxidation in the cells and organisms tested [17]. Oxidative stress is the major factor that could induce related diseases associated with imbalanced ROS and antioxidant defenses. The nanoparticles cause cytotoxicity and antimicrobial activity by causing oxidative distress via the indirect production of reactive oxygen species (ROS) [18]. Metallic nanoparticles such as Ag NPs and Au NPs are exhibited excellent behavior as antioxidants, which act as free radical scavengers [19]. In addition, metallic oxides like ZnO NPs may act as free radical scavengers due to the formation of oxygen vacancies in their lattice structures [20]. Recently, quantum dots have shown promising characteristics due to their advantaged photoluminescence, electroluminescent characteristics, and simple performance with anticancer agents [21].

Using natural sources instead of harmful chemicals in synthesizing nanoparticles is one of the essential requirements for preserving the environment. In addition, the use of biosynthesized nanoparticles may have significant biological compatibility, as indicated by many relevant studies. Thus, it is imperative to investigate environmentally friendly approaches to nanoparticle technology to explore their characteristics and applications, especially in the biological, medicinal, and pharmaceutical fields. For these reasons, in the current work, an aqueous extract of *Hibiscus sabdariffa*, also known as roselle, is an ideal crop used in pharmaceutical and food industries in countries such as China and India [22]. *Hibiscus Sabdariffa* (roselle) is a tall, woody tropical plant with a single stem that belongs to the Malvaceae family and has red Calyces blossoms. Roselle has gotten much interest as a possible source of natural food coloring, medications, and cosmetics [23]. As previously reported, aqueous *Hibiscus sabdariffa* flowers extract is a rich source of anthocyanin and various phytochemicals such as terpenoids, alkaloids, tannins, flavonoids, phenolics, and saponins [24]. These phytochemicals are available in all plant parts, especially leaves and flowers. These phytochemicals are well known for their significant antioxidant and anti-inflammatory properties. They may have many reducing/stabilizing characteristics, exhibiting them as promising candidates for the biosynthesis of ZnO and Au/ZnO NPs [25, 26]. This work's novelty is based on using a low-cost and eco-friendly approach utilizing an aqueous extract of *Hibiscus sabdariffa* flowers to fabricate Au/ZnO NPs as an anticancer and antioxidant agent. This study is the first work on synthesizing Au/ZnO NPs via a green synthesis route using *Hibiscus sabdariffa* flower extract, adopting a hydrothermal extraction method.

In this work, we used an aqueous extract of the *H. Sabdariffa* plant to prepare ZnO, Au, and Au/ZnO nanoparticles. Their optical, structural, and morphological properties were diagnosed by UV–Vis, FTIR, XRD, FESEM, EDX, TEM, and BET techniques. They tested their cytotoxicity in MCF-7 cells and their role in causing oxidative stress by studying their effect on the activities of antioxidant enzymes and testing the lipid peroxidation and calcium levels of MCF-7 cells after exposure to the IC50 dose.

2 Materials and methods

2.1 Materials

Zinc acetate dihydrate Zn $(C_2H_3O_2)_2$. $2H_2O$, sodium hydroxide, and silver nitrate were obtained from Merck,

Germany. Gold (III) chloride trihydrate was obtained from Fluka. Ethylenediaminetetraacetic acid (EDTA). 3-(4,5-dimethylthiazol-2-yl)-2,5-diphenyl tetrazolium bromide (MTT) Sigma-Aldrich. Dulbecco's modified eagle medium (DMEM) and Pen-Strep Fungizone (PSF) were obtained from Gibco, USA. Trypsin (Gibco, Invitrogen, Waltham, MA, USA). Fetal bovine serum (FBS) from Bio-West S.A.S., Nuaille, France). Calcium Assay Kit (Abcam, ab102505). The kits used for measuring MDA, CAT activity assay, SOD activity assay, and GPx activity assay were obtained from TPR, Kushan zist, Iran. Rest substances were obtained from Scharlau.

2.2 Synthesis of ZnO NPs

The dried *Hibiscus sabdariffa* flower (roselle) was ground into a fine powder. Ten grams of drying powder was weighed and added to 100 mL of distilled water. It was stirred while heated to 50 °C at 150 rpm for 30 min. After the extract was brought down to room temperature, it was separated via centrifugation at 3000 rpm for 15 min, filtered by Whatman paper No.1, and stored for subsequent use [23].

ZnO NPs were produced by combining 100 mL of distilled water with 4 g of $Zn(C_2H_3O_2)_2.2\ H_2O$; after the salt had wholly dissolved, 5 mL of roselle flower extract was added to the solution at 70 °C, and 2 M of NaOH was added until the solution's pH reached 12. The reaction mixture was stirred at 250 rpm for 4 h. Afterward, after 20 min of centrifuging the mixture at 6000 rpm, precipitates were produced, washed three times with distilled water and ethanol, then dried at 90 °C for 24 h. Furthermore, it calcinated at 300 °C for 4 h [27]. Figure 1 shows the steps for the synthesis of ZnO NPs.

2.3 Synthesis of Au NPs

A total of 100 mL $HAuCl_4.3H_2O$ solution 1.0 mM and 10 mL of the roselle flower extract were mixed at 90 °C for 1 h under 250 rpm, stirring until the solution color altered from red to dark brown, indicating that the generation of Au NPs had occurred. Biogenic Au NPs were extracted from an aqueous solution at 10,000 rpm for 30 min. Distilled water was then used to wash the newly obtained Au NPs. Distilled water was used to disperse the pellets, then placed into Petri dishes and dried overnight in an oven at 50 °C [28].

2.4 Synthesis of Au/ZnO NPs

The early prepared ZnO NPs (1.0 g) were disseminated in 100 mL of 1 mM of $HAuCl_4.3H_2O$ solution, under stirring (250 rpm), in the dark for 30 min. The mixture's temperature was brought up to 90 °C, and the pH was brought to 7.0. Following the disappearance of yellow, which indicated that the adsorption equilibrium of the gold precursor had been gotten on the ZnO NPs, 5 mL of *Hibiscus sabdariffa* solution was added to the suspension, and it was stirred constantly for 4 h. Centrifugation was used to gather the final product (Au/ZnO). The nanocomposites were separated at 6000 rpm for 20 min. The washing deposits were achieved with distilled water and ethyl alcohol to remove the excess extract components, chlorine, and gold ions. The washing was completed after making sure that the supernatant was free of chloride ion by adding of 0.1 M silver nitrate solution, where no white precipitate as silver chloride was formed [26].

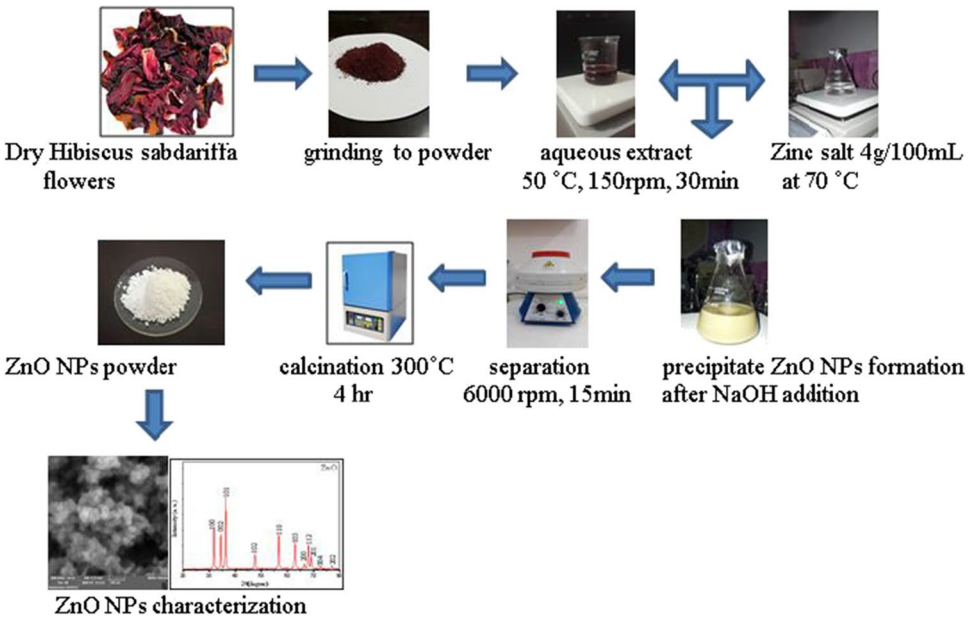

Fig. 1 Graphical abstract for green synthesis of ZnO NPs

2.5 Characterization of the prepared nanomaterials

The nanomaterials were exposed to UV–Vis analysis, ranging from 300 to 800 nm. FTIR spectrum was recorded within 400–4000 cm^{-1} range. X-ray diffraction analysis of the synthesized nanoparticles was recorded using CuK α radiation (1.5406 ˚A) with a range of 20 to 80°. The particle size, shape, and morphology of as-synthesized nanoparticles were analyzed by transmission electron microscope (TEM) and field emission scanning electron microscope (FESEM). BET (Brunauer, Emmett, and Teller) and BJH (Barrett, Joyner, and Halenda) methods were adopted to investigate the surface area and porosity of as fabricated samples. Energy-dispersive X-ray spectroscopy (EDX) technique was employed to examine the elemental distribution in all synthesized nanomaterials.

2.6 In vitro cytotoxicity assay

2.6.1 Cell line culture

Before the study, the MCF-7 cells were grown and kept alive in DMEM. This medium was enhanced with 10% FBS and 1% PSF. At 37 °C, 0.25% trypsin and 0.1% EDTA were added to PBS to detach the cells after reaching 75% confluence. Following this step, the cells were resuspended in DMEM comprising 10% FBS and 1% PSF [29].

2.6.2 Viability cells

MTT assay was achieved to determine the toxic effect of NPs synthesized on the MCF-7 cell line. The 96-well plates were seeded with cells at a density of 5000 cells/well. The plates were then placed in an incubator for 24 h. After being rinsed with PBS (pH 7.4), the cells were cultured for 48 h in a fresh medium comprising various concentrations of ZnO, Au, and Au/ZnO NPs (500, 250, 125, 62.5, 31.25, 15.625, and 7.8125 µg/mL). After 48 h of incubation at 37 °C, 5% carbon dioxide, and a humid atmosphere, a 10-µL solution of recently prepared 5 mg/mL MTT in PBS was added to each well and incubated for an additional 4 h. The formazan was dissolved in 100 µL of (dimethyl sulfoxide) DMSO by gently shaking it at 37 °C. The absorbance of the solution was then measured at 570 nm using an ELISA reader. The results were reported as the average outcomes of six separate experiments. After that, the concentrations of substances that caused a fifty percent decrease in cell viability (IC50) were determined [30]. IC50 was calculated by drawing absorbance against a logarithmic concentration.

2.7 Biochemical analysis

MCF-7 cells were then re-suspended in DMEM comprising 10% FBS and 1% PSF and seeded onto the 24-well plates at a density of 1×10^5. The cells were incubated in a fresh medium containing IC50 of ZnO, Au, and Au/ZnO NPs. After 48 h, the cells were gathered and washed with PBS. Cells were dissociated by cell lysis buffer and centrifugation at 12,000 rpm for 10 min. The supernatant was separated and utilized to measure the calcium levels, MDA levels, CAT, SOD, and GPx activities following the kit manufacturers' instructions [31].

3 Results and discussion

3.1 Green synthesis of ZnO, Au, and Au/ZnO nanoparticles

Adding extract of *H. sabdariffa* flower to Zn $(CH_3COO)_2$. $2H_2O$ solution caused the aqueous solution to undergo physicochemical transformations. In the current study, the formation of ZnO NPs was deduced from the mixture's color shift, which turned from blue to white-yellowish. Flavonoids and phenolic substances cause the conversion of zinc ions into ZnO NPs, and the color of the solution stopped shifting to indicate that the bioreduction of zinc salt into NPs was finished. The previous observations of color differences in the plant-based synthesis of ZnO NPs were confirmed by these results, which were well-matched with the literature [32].

During the synthesis of Au NPs, the alteration in the color of the solution, which took 10 min to go from a light red to a dark purple, was the factor that determined whether or not colloidal Au NPs were created. In previous experiments, the fabrication of the Au NPs took place over a variety of periods. The production time was 2 h when *Polyscias scutellaria* leaf extract was used [33] and 30 min when *Hibiscus sabdariffa* flower extract was used [34]. This may have something to do with the concentration of the extract components that are already there and are responsible for reducing the metal ion.

Au/ZnO NPs preparation was accomplished by a green deposition approach involving extracting *Hibiscus sabdariffa* flowers. The primary purpose of plant extract is the reduction of Au^{3+} to Au^0 and as a capping agent. In the alkaline solution, the ZnO surface acquire negative charges, which enhance the attraction of positively charged gold ions resulting in more significant gold loading [35].

3.2 NPs characterization

3.2.1 UV–Vis analysis

Figure 2 shows the absorption peak of ZnO NPs found at 376 nm. Previous studies have shown that ZnO nanoparticles

exhibit an absorption peak between 340 and 380 nm, demonstrating surface plasmon resonance (SPR). Several earlier investigations have reached the same conclusion [36]. The spectra showed no additional peaks, which indicates the extraordinary purity and crystallinity of the ZnO NPs. The optical features of Au/ZnO NPs nanomaterials were studied via UV–Vis spectroscopy, as seen in Fig. 2, which revealed that the Au/ZnOs have a peak at 376 nm and an additional weak peak at 530 nm. The SPR band of the metallic causes this second peak (Au^0) formed using the *Hibiscus sabdariffa* flower extract as a reducing agent. This lends credence to the hypothesis that the ZnO lattice does not contain any gold species because the impurity would have caused the edge of the absorption spectrum to move to a longer wavelength [37].

UV- vis spectroscopy can effectively determine the production and stability of Au NPs. It was discovered that the band corresponding to the gold SPR occurred at 523 nm. If the particle size is decreased, the maximum wavelength will decrease; this is referred to as a blue shift (Fig. 2) [38].

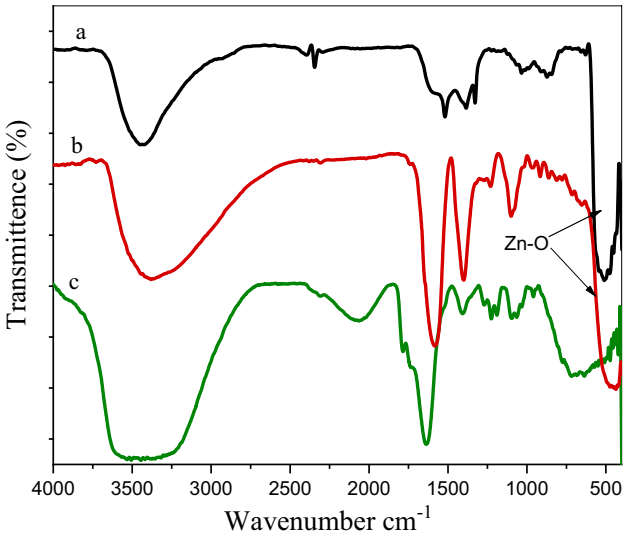

Fig. 3 FTIR spectra of green synthesized **a** ZnO NPs, **b** Au/ZnO NPs, and **c** *Hibiscus sabdariffa* flower extract

3.2.2 FTIR analysis

As shown in Fig. 3, the FTIR spectra of the extract of *Hibiscus sabdariffa* exhibited three distinct vibration bands. It was determined that the stretching vibration of the phenolic hydroxyl group was responsible for the broad and robust band at 3443 cm^{-1}. The (C–C) stretching vibration was accountable for the weak band located at 2065 cm^{-1}. The (C = O) stretching band was determined to be responsible for the signal at 1637 cm^{-1}.

The stretching vibrations of the OH groups are responsible for producing the absorption peak located at 3425.69 cm^{-1}. The presence of nitro groups can be inferred from two prominent peaks at 1519.96 cm^{-1} and 1385 cm^{-1}. There is an absorption band at 532 and 555 cm^{-1} in FTIR spectra ZnO and Au/ZnO NPs; this absorption band represents the typical signal of the Zn–O bonding, which verifies that the material that was synthesized was, in fact, ZnO [39].

Additionally, the peaks at 1639 cm^{-1} in spectra of ZnO and Au/ZnO NPs can be connected with the stretching vibration of the carbonyl groups. The bands at 1033 cm^{-1} and 1014 cm^{-1} are related to (C–O) [40], but the band at 719 cm^{-1} represented the out-of-plane bending of an aromatic (C–H) bond. (C = C) stretching vibrations are responsible for the peaks that appear at 2360 cm^{-1}. R Alfanaar and coworkers recorded 3446.9, 1618.33, and 1101.39 cm^{-1} for (O–H), (C = O), and (C–O–C) bonds, respectively, in the FTIR spectrum of ZnO NPs [26]. These findings shed light on biological molecules' potential role in producing ZnO and Au/ZnO NPs. Flavonoids comprise several different functional groups, one of which is an O–H functional group

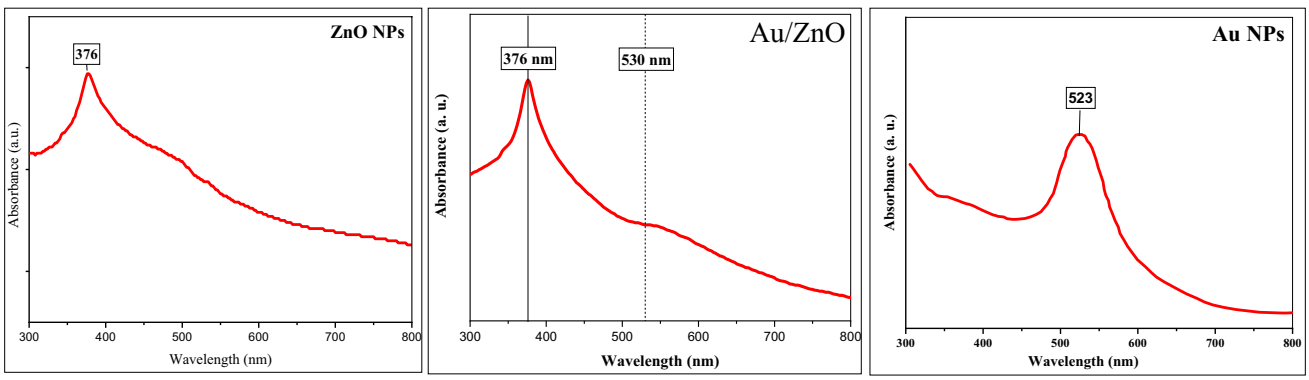

Fig. 2 UV–Vis. The spectrum of biosynthesized ZnO, Au/ZnO, and Au NPs

in forming zinc oxide nanoparticles, and this bond is essential for reducing metal ions [41].

3.2.3 XRD results

The XRD test of the ZnO NPs using *Hibiscus sabdariffa* flower extract can be seen in Fig. 4. The 2θ values of XRD at 31.83°, 34.46°, 36.31°, 47.56°, 56.67°, 62.88°, 66.41°, 67.96°, 69.11°, 72.64°, and 76.97° were assigned to (100), (002), (101), (102), (110), (103), (200), (112), (201), (004), and (202) planes, respectively. All the diffraction peaks were indexed in the ZnO wurtzite structure (JCPDS card 36–1451) [31]. These findings were consistent with the XRD patterns of green synthesized ZnO NPs by *orange fruit peel* extract [41] and *Capparis zeylanica* leaf extract [42]. The biosynthesized ZnO NPs appeared to have a high degree of crystallization, as evidenced by their sharp and narrow peaks. In addition, XRD analysis revealed that ZnO NPs were devoid of contaminants since the only peaks identified on the spectrum were those associated with zinc oxide. Using the Debye–Scherrer equation, we determined the diameter of the ZnO crystallites. The crystallite size is 29 nm for ZnO and Au/ZnO, as determined by Bragg's diffraction angle and the full width at half-maximum (FWHM) of more intense peaks corresponding to (101) planes situated at location 36.31° for ZnO and Au/ZnO NPs.

The XRD patterns for Au/ZnO showed extra XRD peaks denoted by the symbol "#." In Fig. 4, XRD revealed significant peaks at 38.16° and 44.21° for Au/ZnO. These peaks correspond to the (111) and (200) planes of the face-centered cubic (FCC) structure of Au, respectively (JCPDS Card No. 65–2870) [14]. Because there was no alteration in the peak position of the ZnO NPs, it was clear that the Au NPs had only been deposited on the ZnO NPs, and they had not penetrated the lattice of the ZnO NPs. The XRD pattern of the Au/ZnO is remarkably analogous to that of the pure ZnO NPs; this indicates that the creation of Au NPs during the reaction does not affect the crystal structure of ZnO [11]. While R Alfanaar et al. and coworkers determined the two peaks location corresponding to 111 and 200 at 36.3° and 47.5°, this difference may be attributed to the difference in the amount of gold added and volume of extract in both studies [26].

The XRD pattern for the Au NPs synthesized utilizing an aqueous extract of *Hibiscus sabdariffa* flower in Fig. 4 shows intense diffraction peaks at 2θ° of 37.9°, 44.11°, 64.32°, and 77.37°, which corresponds to the (111), (200), (220), and (311) (JCPDS no. 01–1174) [43] planes of Bragg reflections of FCC structure of Au NPs. From the calculations, the average particle sizes of synthesized Au NPs were 9.7 nm, from the peak corresponding to (111) planes positioned at 37.9°.

3.2.4 FESEM, EDX, and TEM analysis

The FESEM offered further insight into the size, shape, and surface morphology of the ZnO, Au, and Au/ZnO NPs revealed with the FESEM image, as shown in Fig. 5. Structural characterizations reveal that the synthesized products had a nano-sized range, irregular, almost spherical, with an average size of 50.7 nm, their size ranged from 21 to 89 nm (using the ImageJ program, select 200 particles for this purpose (Fig. 6a). Similar to the other metallic nanomaterials, which have been manufactured utilizing green synthesis methodologies, a tendency to aggregate is seen for ZnO NPs [44].

EDX spectra were performed on both the ZnO and Au/ZnO NPs to conclude the composition of the elemental distribution in both sample. The elemental profile showed peaks with Zn characteristics at (1, 8.6, 9.6) keV, which validated the generation of ZnO NPs. Simultaneously, the peak for oxygen can be seen at 0.5 keV. As shown in Fig. 7, the atomic percentages of the elements demonstrate that zinc is the essential component, constituting 61.13% of the overall composition, along with oxygen at 38.87%, which also verifies the excellent purity of the produced ZnO NPs; this conforms with the findings obtained by the green synthesis of ZnO NPs [45]. Moreover, the two peaks of gold are displayed at 2.2 and 9.8 keV. The nanocomposite containing

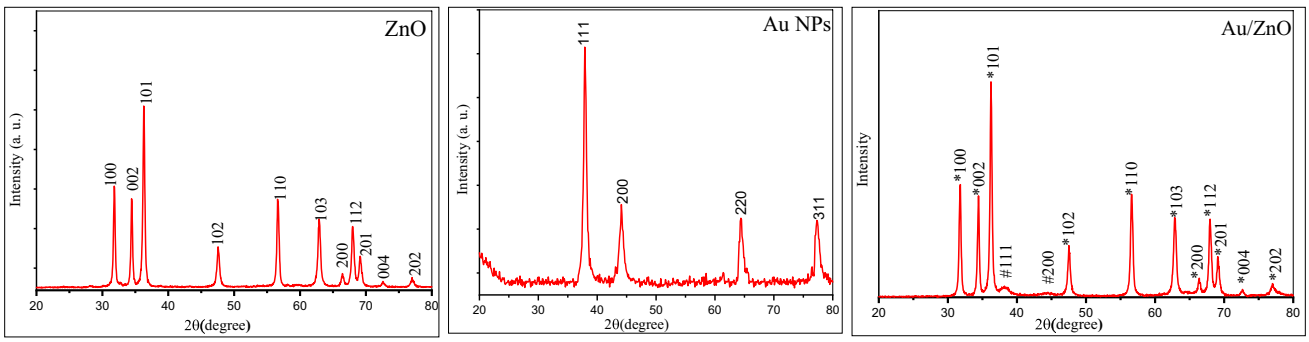

Fig. 4 XRD diffractograms of biosynthesized ZnO, Au, and Au/ZnO NPs. (#) denotes peaks of gold in Au/ZnO diffractogram

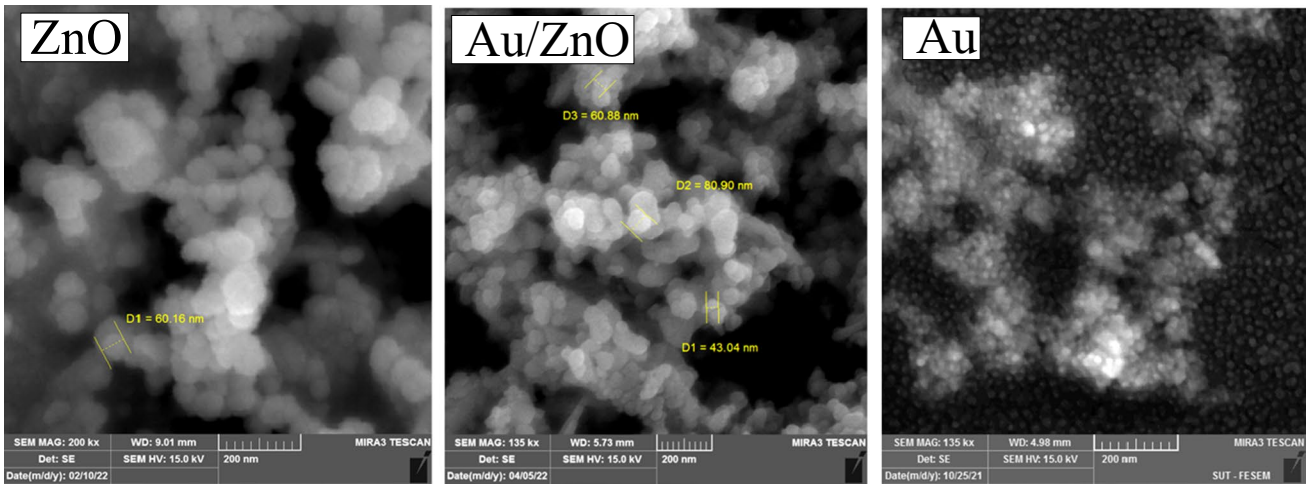

Fig. 5 FESEM micrograms of biosynthesized ZnO, Au/ZnO, and Au NPs

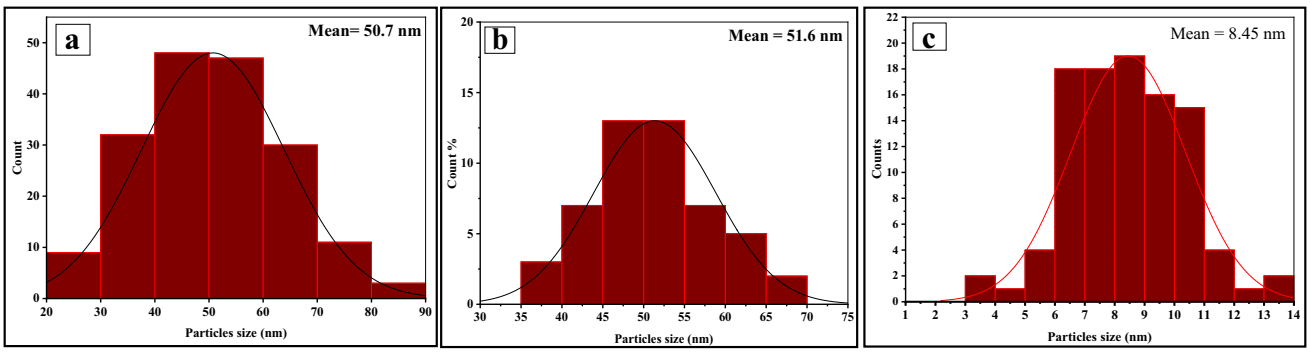

Fig. 6 Particle size distribution histograms for **a** ZnO NPs, **b** ZnO NPs, and **c** Au NPs estimated from FESEM images

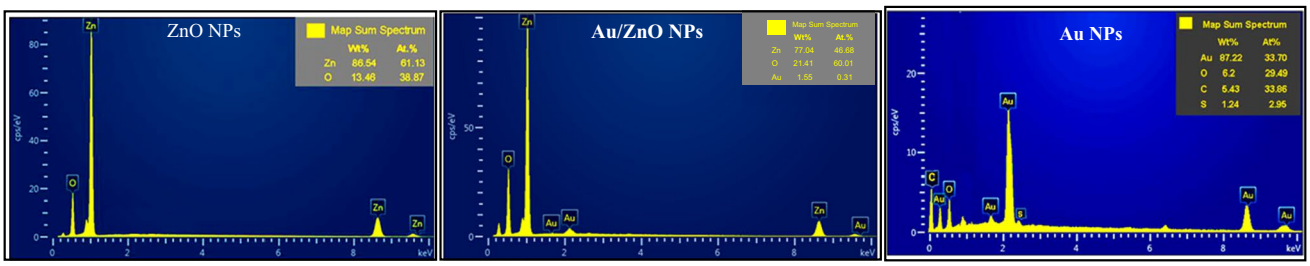

Fig. 7 EDX spectra of biosynthesized ZnO, Au/ZnO, and Au NPs

Au/ZnO has a gold content ratio of 1.55% (w/w). The EDX spectrum in Fig. 7 suggests that the nanoparticles have a high purity because gold, zinc, and oxygen are the only discovered elements. The EDX spectra do not contain extra peaks [11].

In Fig. 7, the EDX spectrum of Au NPs demonstrated the existence of the Au at ratios of 87.22%(wt %) and 33.70%(At %). In other words, the robust signal from the gold atoms demonstrates the successful synthesis of the Au NPs. This EDX profile includes other signals, such as C, O, and S, which were also found, they emanated from organic biomolecules or phenolic compounds attached to the surface of Au NPs [43].

The TEM was utilized to visualize the nanoparticles' shape and diameter. The TEM examination determined that the average diameter of the NPs is 51.6 nm, as seen in Fig. 6b, which is about the same as the size calculated by the FESEM analysis. TEM pictures of ZnO NPs showed

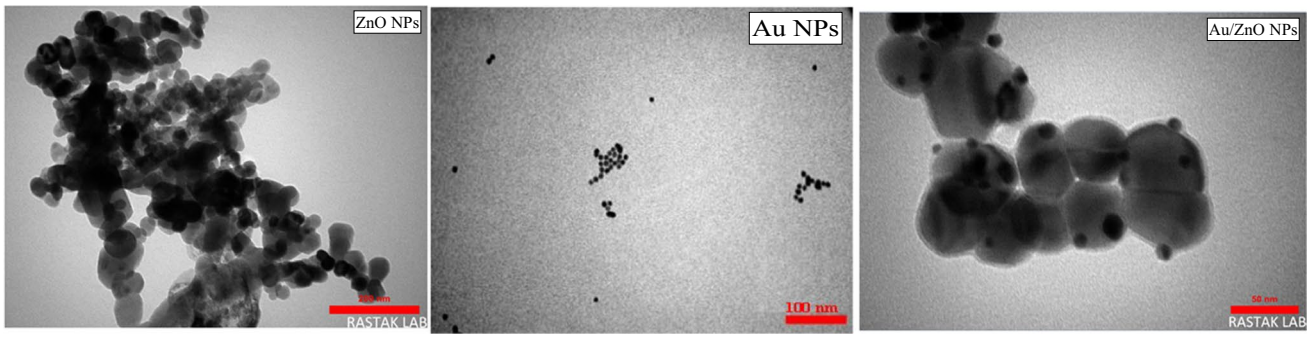

Fig. 8 The TEM micrograms of biosynthesized ZnO, Au/ZnO, and Au NPs

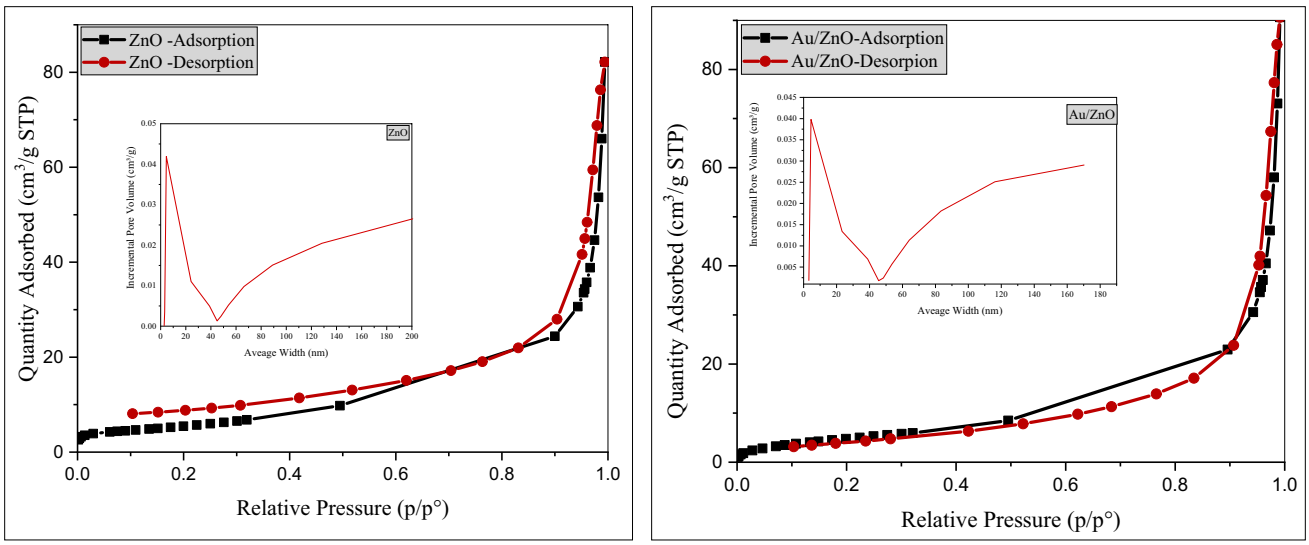

Fig. 9 N_2 adsorption–desorption isotherms and the matching pore size distribution curve of biosynthesized ZnO and Au/ZnO NPs

nanoparticles with various spherical forms, some of which were irregular, as seen in Fig. 8. What distinguishes the shapes of the Au/ZnO composites is that gold nanoparticles are not seen independently, which indicates the deposition of most of the added gold at the zinc oxide surface.

The morphology of the Au NPs seen there is spherical. Particles of almost uniform sizes, well dispersed with diameters ranging from 3 to 14 nm, were produced during the formation process. The TEM investigation concluded that the average particle size was 8.45 nm, as shown in Fig. 6c.

3.2.5 Surface area and pores size analysis (BET, BJH)

The N_2 adsorption–desorption isotherm of the ZnO and Au/ZnO NPs can be seen in Fig. 9, and the related BJH pore size distribution can be seen in the insets of those figures. As Table 1 illustrates, the adsorption–desorption properties of type IV, as specified by the IUPAC classification [46], which is characteristic of mesoporous materials, are reflected in the isotherms for two samples. ZnO NPs had a specific surface area of 20.21 m^2/g, while Au/ZnO NPs had an average specific surface area of 19.23 m^2/g; the decrease may be a product of Au NPs deposited in pores of ZnO NPs.

Table 1 Surface area study (BET, BJH) of ZnO and Au/ZnO NPs

Property	ZnO	Au/ZnO
Surface area (m^2/g)	20.21	19.23
Pore volume (cm^3/g)	0.050046	0.050722
Pore diameter (nm)	9.91	10.56
Isotherm type	IV	IV
Hysteresis (p/p_o)	H3	H3
Type of pore	Mesoporous	Mesoporous

3.3 Cytotoxicity analysis and viability of cells

According to the findings of several studies, nanoparticles have the potential to serve as helpful therapeutic agents in the treatment of a range of cancers [47]. The cytotoxicity of ZnO, Au, and Au/ZnO NPs on MCF-7 cells was evaluated with MTT assays, and the IC50 values were determined to be 33.5, 28.7, and 34.9 µg/mL, respectively, as shown in Fig. 10.

Many factors determine the IC50 value, including the nature of nanoparticles and their size, shape, and capping agents, also included as the internal and external environment of cells. The findings presented here are in line with those found in earlier research, which found that ZnO NPs exhibited significant cytotoxicity toward cancer cells such as MG-63, Saos-2 [34], MCF-7 [48], and the colorectal cancer cell HT 29 [49].

It has yet to be determined how precisely ZnO (also Au) NPs exert their cytotoxicity. According to one hypothesis, the intracellular release of dissolved [Zn^{2+}], followed by ROS generation, is the primary mechanism behind the cytotoxicity caused by ZnO NPs. The Zn^{2+} released from particles might disrupt the homeostasis of cells. The dissolution process is ongoing and influenced by various factors, including shape, surface area, crystallinity, and others [50].

There are few studies in this field concerning the toxicity of the compound Au/ZnO NPs. The results obtained from this study indicate lower toxicity than the ZnO NPs, as the value of IC50 reached 34.9 µg/mL. Composites of other elements deposited on zinc oxide showed cytotoxicity when treated with human liver adenocarcinoma cells (HepG2 cells), including Fe/ZnO, Ag/ZnO, Pd/ZnO, and Co/ZnO NPs, under UV irradiation, the results demonstrated that the NPs displayed cytotoxicity against HepG2 cells, with IC50 of 42.60, 37.20, 45.10, 77.20 and 56.50 µg/ml, respectively [51]. In Fig. 10, we observe that Au/ZnO NPs cytotoxicity is less than ZnO and Au NPs, especially after 31.25 g/mL concentration, so that it can be used as a drug carrier agent.

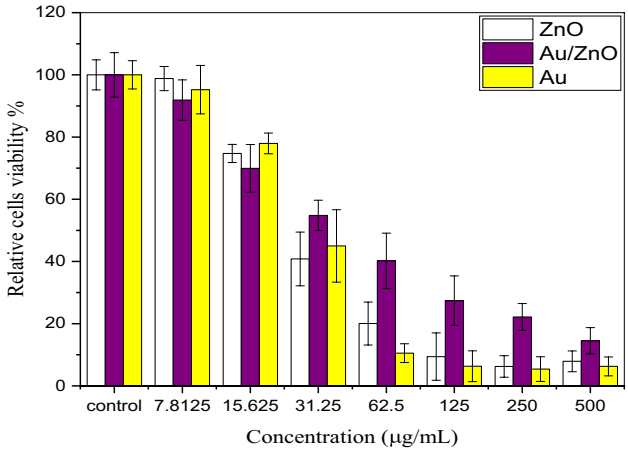

Fig. 10 MTT assay results confirm the in vitro cytotoxicity of ZnO, Au, and Au/ZnO NPs towards MCF-7 cells for 48 h. Values are mean ± SD of six separate experiments

3.4 Calcium levels

The amount of free calcium was measured to determine whether or not changes in intracellular calcium ions were involved in the apoptosis produced by ZnO, Au, and Au/ZnO NPs. Thus, increases in cytoplasmic calcium levels result in mitochondrial dysfunction and apoptosis [52]. In the MCF-7 cells treated with the IC50 concentration of ZnO, Au, and Au/ZnO NPs, it was revealed that the amount of free cytoplasmic Ca^{2+} had increased by 33, 9.7, and 6.9%, respectively, compared with control cells, as shown in Fig. 11.

In 2020, H. Zhang and coworkers demonstrated that out of 24 different types of metal oxides, the CuO and ZnO nanoparticles caused a greater intracellular calcium flow than the other types of metal oxides nanoparticles, which did not feature as prominently [53]. Intracellular calcium [Ca^{2+}] triggers essential cellular activities such as metabolic regulation and mitotic division, thereby regulating the process of cell death [54].

3.5 Lipid peroxidation (LP)

MDA is the result of the oxidation of lipids. As a result, it is a sign that the cells have been damaged due to oxidative stress. In this work, MCF-7 cells were exposed to IC50 of ZnO, Au, and Au/ZnO NPs; the treatment increased MDA levels compared to the untreated cells. The values of MDA recorded for the synthesized nanoparticles were 2.91, 3.57, and 2.85 µM for ZnO, Au, and Au/ZnO NPs, respectively, as presented in Fig. 11; these values were compared to the value recorded for the control cell, which was 0.39 µM. Other studies went in this direction; in 2017, S. Chakraborti and coworkers noted a significant increase in the MDA level after 2 h of treatment of MCF-7 cells with ZnONPs [55]. The cells treated with ZnO NPs had a significantly elevated level of MDA; at the same time, the antioxidants GPx and SOD levels were dramatically reduced, indicating an oxidative effect [56]. The researcher, T. Rao et al., tested a composite of another type (Ag/TiO_2) that also showed an apparent influence on the growth inhibition of MCF-7 cells and raised it to the level of MDA in a manner proportionate with the concentration of the composite [57].

3.6 CAT, GPX, and SOD activity

CAT plays a significant role in enzymatic oxidant defense by protecting the cell from H_2O_2 by transforming them into O_2 and H_2O [58]. After exposing MCF-7 cells to ZnO, Au,

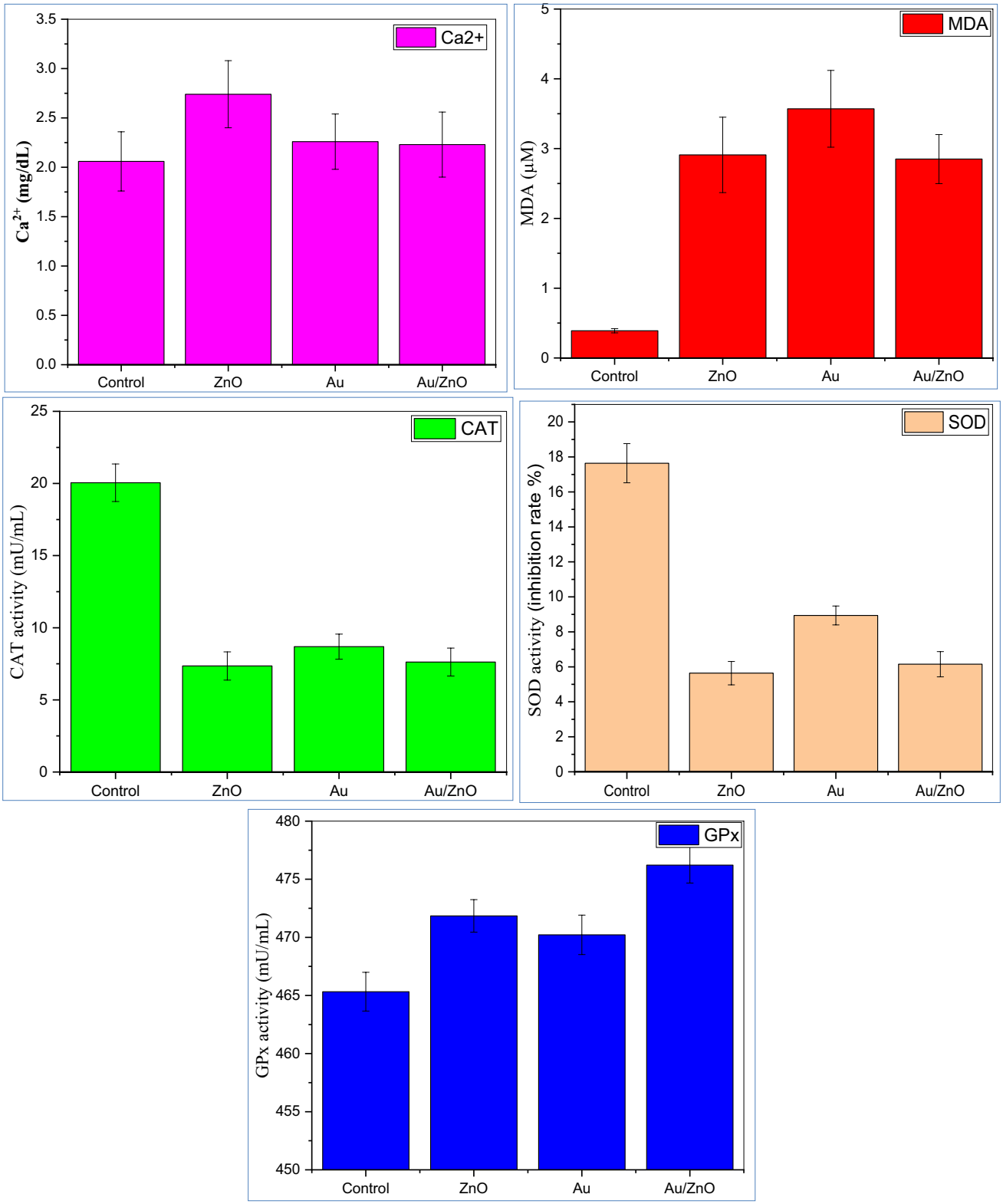

Fig. 11 Shows an increase in levels of [$Ca.^{2+}$] and MDA, as well as reduces in the enzyme activity CAT, SOD, and GPx after exposure to MCF-7 cells to IC50 dose of NPs synthesis for 48 h. (The results are denoted by the mean ± SD of three separate experiments)

Table 2 Results of MDA and Ca^{2+} levels and CAT, SOD, and GPx activities in MCF-7 cell lines after being treated with IC50 ZnO, Au, and Au/ZnO NPs

Tests	Control	ZnO	Au	Au/ZnO
MAD (μM)	0.39	2.91	3.57	2.85
Ca^{2+} (mg/dL)	2.06	2.74	2.26	2.22
CAT (mU/mL)	20.05	7.35	8.69	7.62
SOD (mU/mL)	17.64	5.64	8.94	6.15
GPx (mU/mL)	465.33	471.85	470.22	476.22

and Au/ZnO NPs, the CAT activity in the MCF-7 cells was shown to be altered. The levels of CAT activity recorded at IC50 concentration of ZnO, Au, and Au/ZnO NPs were 7.35, 8.69, and 12.83 nmol/min/mL, respectively, compared to 20.05 nmol/min/mL for the control group (Fig. 11). In other words, the CAT activity was reduced by about 63%, 55%, and 62% for ZnO, Au, and Au/ZnO NPs, respectively.

SODs play the primary role in antioxidant defense regulations by catalyzing the dismutation of superoxide anion free radical (O^{2-}) into O_2 and (H_2O_2) [59]. The experimental results in the current study were recorded at 5.64, 8.94, and 6.15 mU/mL for the ZnO, Au, and Au/ZnO NPs, respectively, when compared to the control group, which recorded 17.64 mU/mL. The results indicate a decrease in the SOD activity by 68%, 49%, and 65% for ZnO, Au, and Au/ZnO NPs, respectively, compared to the control group.

GPx is employed in cells' defense against oxidative stress by catalyzing the reduction of hydroperoxides by reduced GSH [60]. As displayed in Table 2, the results of the current work suggested a slight increase in the activity of the GPx compared with the control cells, which were 471.85, 468.59, 476.22, and 465.33 mU/mL for ZnO, Au, Au/ZnO NPs, and the control cells, respectively (see Table 2).

Lower levels of CAT activity may also correspond to enzyme inhibition due to higher degrees of stress from higher concentrations of produced NPs. This may be related to the possible generation of peroxyl radicals, which are known to impede the actions of CAT and SOD [56]. Accordingly, numerous investigations have described lower enzyme catalase levels in tumors and cancer cell lines compared to healthy cells. There is still much mystery about this impairment in cancer cells. However, researchers described a few hypotheses to try and explain it, such as hypermethylation of catalase promoter or the involvement of transcription factors [61]. It also may be due to high levels of reactive oxygen species that oxidative proteins and lead to breakdown by denaturation.

The results of other studies are consistent with the current study's findings. When HeLa cells were exposed to ZnO NPs, this decreased the activity of the enzymes GPx, CAT, and SOD [62]. The ZnO NPs suppressed the expression of antioxidant-related genes (SOD and CAT) in the male mice [63]. ZnO NPs markedly decreased the enzyme's activities of SOD and GPX and the GSH level. The results inferred that ZnO NPs might induce oxidative stress in mouse GC-1 spg cells by leading to an imbalance between the cellular antioxidant defense system and ROS production [64].

4 Conclusions

This work used roselle extract to prepare ZnO, Au, and Au/ZnO NPs as environmentally friendly. FESEM images approve the formation of nanosized ZnO, Au, and Au/ZnO NPs, whereas XRD diffraction graphs confirm crystal structure formation with high purity. By Scherrer's equation, the average crystal size was 50.7, 8.45, and 50.63 nm for ZnO, Au, and Au/ZnO, respectively.

In vitro anticancer activity of ZnO, Au, and Au/ZnO has been investigated in MCF-7 cell lines. Experimental findings indicate that the cytotoxicity effects of synthesized NPs primarily depended on the concentrations used. The value of IC_{50} is 33.5, 28.7, and 34.9 μg/mL for ZnO, Au, and Au/ZnO NPs, respectively. Flow cytometry results confirmed that ZnO, Au, and Au/ZnO NPs induce apoptosis in MCF-7 cells. The values of MDA recorded were 2.91, 3.57, 2.85, and 0.39 μM for ZnO, Au, Au/ZnO NPs, and the control cell, respectively, as well as the results revealed that the amount of free cytoplasmic Ca^{2+} had increased of 33, 9.7, and 6.9%, respectively, compared with control cells.

In addition, exposing MCF-7 cells to ZnO, Au, and Au/ZnO NPs caused an imbalance in the antioxidant enzymes, represented by a reduction in the activity of enzymes CAT and SOD compared to untreated cells. The CAT activity was reduced by about 63%, 55%, and 62% for ZnO, Au, and Au/ZnO NPs, respectively, as well as the results indicate a decrease in the SOD activity by 68%, 49%, and 65% for ZnO, Au, and Au/ZnO NPs, respectively when compared to the control group. Consequently, Au/ZnO NPs may be suggested cytotoxic activity, an inhibitor effect on the antioxidant system, and an oxidative stress inducer.

Author contribution Qasim R. Shochah: methodology, investigation, software, formal analysis, writing — original draft, visualization, and formal analysis. Ferdous A. Jabir: writing — review and editing, supervision, project administration, and resources.

Data availability Not applicable.

Code availability Not applicable.

Declarations

Ethics approval Not applicable.

Consent to participate Not applicable.

Consent for publication Not applicable.

Conflict of interest The authors declare no competing interests.

References

1. Sung H, Ferlay J, Siegel RL et al (2021) Global cancer statistics 2020: GLOBOCAN estimates of incidence and mortality worldwide for 36 cancers in 185 countries. CA Cancer J Clin 71:209–249. https://doi.org/10.3322/caac.21660
2. Razavi R, Amiri M, Alshamsi HA, Eslaminejad T, Salavati-Niasari M (2021) Green synthesis of Ag nanoparticles in oil-in-water nano-emulsion and evaluation of their antibacterial and cytotoxic properties as well as molecular docking. Arab Chem 14:103323
3. Jaganjac M, Sunjic SB, Zarkovic N (2020) Utilizing iron for targeted lipid peroxidation as anticancer option of integrative biomedicine: a short review of nanosystems containing iron. Antioxidants 9:1–16. https://doi.org/10.3390/antiox9030191
4. Xin Z, He Q, Wang S, Han X, Fu Z, Xu X, Zhao X (2022) Recent progress in ZnO-based nanostructures for photocatalytic antimicrobial in water treatment: a review. Appl Sci 12:7910. https://doi.org/10.3390/app12157910
5. Li N, Chen Y, Zhang YM et al (2014) Polysaccharide-gold nanocluster supramolecular conjugates as a versatile platform for the targeted delivery of anticancer drugs. Sci Rep 4:4164. https://doi.org/10.1038/srep04164
6. Jahangirian H, Kalantari K, Izadiyan Z et al (2019) A review of small molecules and drug delivery applications using gold and iron nanoparticles. Int J Nanomed 14:1633–1657. https://doi.org/10.2147/IJN.S184723
7. Elsayed KA, Alomari M, Drmosh QA, Alheshibri M, Al Baroot A, Kayed TS, Manda AA, Al-Alotaibi AL (2022) Fabrication of ZnO-Ag bimetallic nanoparticles by laser ablation for anticancer activity. Alex Eng J 61(2):1449–1457. https://doi.org/10.1016/j.aej.2021.06.051
8. Hong EJ, Sivakumar P, Ravichandran V, Choi DG, Kim Y-S, Shim MS (2019) Pro-oxidant drug-loaded Au/ZnO hybrid nanoparticles for cancer-specific chemo-photodynamic combination therapy. ACS Biomater Sci Eng 5(10):5209–5217. https://doi.org/10.1021/acsbiomaterials.9b01339
9. Anjum S, Nawaz K, Ahmad B, Hano C, Abbasi BH (2022) Green synthesis of biocompatible core–shell (Au–Ag) and hybrid (Au–ZnO and Ag–ZnO) bimetallic nanoparticles and evaluation of their potential antibacterial, antidiabetic, antiglycation and anticancer activities. RSC Adv 12:23845–23859. https://doi.org/10.1039/D2RA03196E
10. Pradeev raj K, Sadaiyandi K, Kennedy A et al (2018) Influence of Mg doping on ZnO nanoparticles for enhanced photocatalytic evaluation and antibacterial analysis. Nanoscale Res Lett 13:229. https://doi.org/10.1186/s11671-018-2643-x
11. Mezni A, Mlayah A, Serin V, Smiri LS (2014) Synthesis of hybrid Au-ZnO nanoparticles using a one pot polyol process. Mater Chem Phys 147:496–503. https://doi.org/10.1016/j.matchemphys.2014.05.022
12. Goudarzi M, Alshamsi HA, Amiri M, Salavati-Niasare M (2021) ZnCo2O4/ZnO nanocomposite: facile one-step green solid-state thermal decomposition synthesis using Dactylopius coccus as capping agent, characterization and its 4T1 cells cytotoxicity investigation and anticancer activity. Arab J Chem 14(9):103316. https://doi.org/10.1016/j.arabjc.2021.103316
13. Raghavendra G (2017) Cell viability studies of green synthesised zno nanoparticles for antibacterial properties. Am J Mater Synth Process 2:56. https://doi.org/10.11648/j.ajmsp.20170205.11
14. Albo Hay Allah MA, Alshamsi HA (2022) Green synthesis of ZnO NPs using *Pontederia crassipes* leaf extract:characterization, their adsorption behavior and anti-cancer property. Biomass Conv Bioref. https://doi.org/10.1007/s13399-022-03091-y
15. Hussain A, Oves M, Alajmi MF et al (2019) Biogenesis of ZnO nanoparticles using: Pandanus odorifer leaf extract: anticancer and antimicrobial activities. RSC Adv 9:15357–15369. https://doi.org/10.1039/c9ra01659g
16. Mauricio MD, Guerra-Ojeda S, Marchio P et al (2018) Nanoparticles in medicine: a focus on vascular oxidative stress. Oxid Med Cell Longev 2018:1–21. https://doi.org/10.1155/2018/6231482
17. Rashdan SA (2021) Chemical detection of the toxicity of nanoparticles of metals and metal oxides. Nano Biomed Eng 13:401–413. https://doi.org/10.5101/nbe.v13i4.p401-413
18. Alavi M, Hamblin MR, Martinez F, Kennedy JF, Khan H (2022) Synergistic combinations of metal, metal oxide, or metalloid nanoparticles plus antibiotics against resistant and non-resistant bacteria. Micro Nano Bioaspects 1(1):1–9
19. Alavi M, Kowalski R, Capasso R, Coutinho HDM, de Menezes IRA (2022) Various novel strategies for functionalization of gold and silver nanoparticles to hinder drug-resistant bacteria and cancer cells. Micro Nano Bioaspects 1(1):38–48
20. Anzabi Y (2018) Biosynthesis of ZnO nanoparticles using barberry (Berberis vulgaris) extract and assessment of their physicochemical properties and antibacterial activities. Green Processing Synth 7:114–121
21. Alavi M, Webster TJ, Li L (2022) Theranostic safe quantum dots for anticancer and bioimaging applications. Micro Nano Bioaspects 1(2):1–11
22. Izquierdo-Vega JA, Arteaga-Badillo DA, Sánchez-Gutiérrez M, Morales-González JA, Vargas-Mendoza N, Gómez-Aldapa CA, Castro-Rosas J, Delgado-Olivares L, Madrigal-Bujaidar E, Madrigal-Santillán E (2020) Organic acids from roselle (*Hibiscus sabdariffa* L.)-a brief review of its pharmacological effects. Biomedicines 8(5):1–16
23. Chumsri P, Sirichote A, Itharat A (2008) Studies on the optimum conditions for the extraction and concentration of roselle (Hibiscus sabdariffa Linn.) extract. Songklanakarin J Sci Technol 30:133–139
24. Abdallah EM (2016) Antibacterial efficiency of the Sudanese roselle (Hibiscus sabdariffa L.), a famous beverage from Sudanese folk medicine. J Intercult Ethnopharmacol 5(2):186–90. https://doi.org/10.5455/jice.20160320022623
25. Alshamsi HA, Jaffer AA (2022) New Hibiscus sabdariffa L petals extract based green synthesis of zinc oxide nanoparticles for photocatalytic degradation of rhodamine B dye under solar light. AIP Conf Proc 2394:040017. https://doi.org/10.1063/5.0121228
26. Alfanaar R, Elim PE, Kesuma RF, Monica E (2019) Synthesis of ZnO-gold nanoparticles composite using Hibiscus sabdariffa extract as reductor. J Phys Conf Ser 1307:1–7. https://doi.org/10.1088/1742-6596/1307/1/012006
27. Lau GE, Abdullah CAC, Ahmad WANW et al (2020) Eco-friendly photocatalysts for degradation of dyes. Catalysts 10:1–16. https://doi.org/10.3390/catal10101129
28. Mishra P, Ray S, Sinha S et al (2016) Facile bio-synthesis of gold nanoparticles by using extract of Hibiscus sabdariffa and evaluation of its cytotoxicity against U87 glioblastoma cells under hyperglycemic condition. Biochem Eng J 105:264–272. https://doi.org/10.1016/j.bej.2015.09.021

29. Dang Z, Sun J, Fan J et al (2021) Zinc oxide spiky nanoparticles: a promising nanomaterial for killing tumor cells. Mater Sci Eng C 124:112071. https://doi.org/10.1016/j.msec.2021.112071
30. Franco-Molina MA, Mendoza-Gamboa E, Sierra-Rivera CA et al (2010) Antitumor activity of colloidal silver on MCF-7 human breast cancer cells. J Exp Clin Cancer Res 29:1–7. https://doi.org/10.1186/1756-9966-29-148
31. Cen J, Zhang L, Liu F et al (2016) Long-term alteration of reactive oxygen species led to multidrug resistance in MCF-7 cells. Oxid Med Cell Longev 2016:7053451. https://doi.org/10.1155/2016/7053451
32. Elsayed MS, Ahmed IA, Bader DMD, Hassan AF (2022) Green synthesis of nano zinc oxide/nanohydroxyapatite composites using date palm pits extract and eggshells: adsorption and photocatalytic degradation of methylene blue. Nanomaterials 12:1–18. https://doi.org/10.3390/nano12010049
33. Yulizar Y, Utari T, Ariyanta HA, Maulina D (2017) Green method for synthesis of gold nanoparticles using Polyscias scutellaria leaf extract under UV light and their catalytic activity to reduce methylene blue. J Nanomater 2017:3079636. https://doi.org/10.1155/2017/3079636
34. Zangeneh MM, Zangeneh A (2020) Novel green synthesis of Hibiscus sabdariffa flower extract conjugated gold nanoparticles with excellent anti-acute myeloid leukemia effect in comparison to daunorubicin in a leukemic rodent model. Appl Organomet Chem 34:1–13. https://doi.org/10.1002/aoc.5271
35. Yazid H, Adnan R, Hamid SA, Farrukh MA (2010) Synthesis and characterization of gold nanoparticles supported on zinc oxide via the deposition-precipitation method. Turkish J Chem 34:639–650. https://doi.org/10.3906/kim-0912-379
36. Kavithaa K, Paulpandi M, Ponraj T et al (2016) Induction of intrinsic apoptotic pathway in human breast cancer (MCF-7) cells through facile biosynthesized zinc oxide nanorods. Karbala Int J Mod Sci 2:46–55. https://doi.org/10.1016/j.kijoms.2016.01.002
37. Abdulhusain ZH, Alshamsi HA, Salavati-Niasari M (2021) Facile synthesis of Au/ZnO/RGO nanohybrids using 1,8-diamino-3,6-dioxaoctan as novel functional agent for photo-degradation water treatment. J Mater Res Technol 5:6098–6112. https://doi.org/10.1016/j.jmrt.2021.11.038
38. Yu J, Xu D, Guan HN et al (2016) Facile one-step green synthesis of gold nanoparticles using Citrus maxima aqueous extracts and its catalytic activity. Mater Lett 166:110–112. https://doi.org/10.1016/j.matlet-.2015.12.031
39. Abdulhusain ZH, Alshamsi HA, Salavati-NiasariGavade M (2022) Silver and zinc oxide decorated on reduced graphene oxide: simple synthesis of a ternary heterojunction nanocomposite as an effective. Int J Hydrog Energy. https://doi.org/10.1016/j.ijhydene.2022.08.018
40. Abbasi BH, Shah M, Hashmi SS et al (2019) Green bio-assisted synthesis, characterization and biological evaluation of biocompatible ZnO nps synthesized from different tissues of milk thistle (Silybum marianum). Nanomaterials 9:0–19. https://doi.org/10.3390/nano9081171
41. Doan Thi TU, Nguyen TT, Thi YD et al (2020) Green synthesis of ZnO nanoparticles using orange fruit peel extract for antibacterial activities. RSC Adv 10:23899–23907. https://doi.org/10.1039/d0ra04926c
42. Nilavukkarasi M, Vijayakumar S, Prathipkumar S (2020) Capparis zeylanica mediated bio-synthesized ZnO nanoparticles as antimicrobial, photocatalytic and anti-cancer applications. Mater Sci Energy Technol 3:335–343. https://doi.org/10.1016/j.mset.2019.12.004
43. Rashki S, Alshamsi HA, Amiri O, Safardoust-Hojaghan H, Salavati-Niasari M, Nazari-Alam A, Khaledi A (2021) Eco-friendly green synthesis of ZnO/GQD nanocomposites using Protoparmeliopsis muralis extract for their antibacterial and anti-biofilm activity. Mol Liq 335:116195. https://doi.org/10.1016/j.molliq.2021.116195
44. Chinnathambi A, Alahmadi TA (2021) Zinc nanoparticles green-synthesized by Alhagi maurorum leaf aqueous extract: chemical characterization and cytotoxicity, antioxidant, and anti-osteosarcoma effects. Arab J Chem 14:103083. https://doi.org/10.1016/j.arabjc-.2021.103083
45. Park JK, Rupa EJ, Arif MH et al (2021) Synthesis of zinc oxide nanoparticles from Gynostemma pentaphyllum extracts and assessment of photocatalytic properties through malachite green dye decolorization under UV illumination-a green approach. Optik (Stuttg) 239:166249. https://doi.org/10.1016/j.ijleo.2020.166249
46. Kim KJ, Kreider PB, Ahn HG, Chang CH (2018) Characterization of cotton ball-like Au/ZnO photocatalyst synthesized in a microreactor. Micromachines 9:1–13. https://doi.org/10.3390/mi9070322
47. Prados J, Melguizo C, Ortiz R et al (2012) Doxorubicin-loaded nanoparticles: new advances in breast cancer therapy. Anticancer Agents Med Chem 12:1058–1070. https://doi.org/10.2174/-18715212803529646
48. Aljaballi AAA, Obeid MA, Bakshi HA, Alshaer W, Ennab RM, Al-Trad B, Alkhateeb W, Al-Batayneh KM, Al-Kadash A, Alsotari S, Nsairat H, Tambuwala MM (2022) Synthesis, characterization, and assessment of anti-cancer potential of ZnO nanoparticles in an in vitro model of breast cancer. Molecules 27(6):1827
49. Bai Aswathanarayan J, Rai Vittal R, Muddegowda U (2018) Anticancer activity of metal nanoparticles and their peptide conjugates against human colon adenorectal carcinoma cells. Artif Cells, Nanomedicine Biotechnol 46:1444–1451. https://doi.org/10.1080/21691401.2017.1373655
50. Aldalbahi A, Alterary S, Ali Abdullrahman Almoghim R et al (2020) Greener synthesis of zinc oxide nanoparticles: characterization and multifaceted applications. Molecules 25:1–14. https://doi.org/10.3390/-molecules25184198
51. Ismail AFM, Ali MM, Ismail LFM (2014) Photodynamic therapy mediated antiproliferative activity of some metal-doped ZnO nanoparticles in human liver adenocarcinoma HepG2 cells under UV irradiation. J Photochem Photobiol B Biol 138:99–108. https://doi.org/10.1016/j.jphotobiol.2014.04.006
52. Rawat PS, Jaiswal A, Khurana A et al (2021) Doxorubicin-induced cardiotoxicity: an update on the molecular mechanism and novel therapeutic strategies for effective management. Biomed Pharmacother 139:111708. https://doi.org/10.1016/j.biopha.2021.111708
53. Zhang H, Ji Z, Xia T et al (2012) Use of metal oxide nanoparticle band gap to develop a predictive paradigm for oxidative stress and acute pulmonary inflammation. ACS Nano 6:4349–4368. https://doi.org/10.1021/nn3010087
54. Lin MY, Cheng WT, Cheng HC et al (2021) Baicalin enhances chemosensitivity to doxorubicin in breast cancer cells via upregulation of oxidative stress-mediated mitochondria-dependent apoptosis. Antioxidants 10(10):1506. https://doi.org/10.3390/antiox10101506
55. Chakraborti S, Chakraborty S, Saha S et al (2017) PEG-functionalized zinc oxide nanoparticles induce apoptosis in breast cancer cells through reactive oxygen species-dependent impairment of DNA damage repair enzyme NEIL2. Free Radic Biol Med 103:35–47. https://doi.org/10.1016/j.freeradbiomed.2016.11.048
56. Liao C, Jin Y, Li Y, Tjong SC (2020) Interactions of zinc oxide nanostructures with mammalian cells: cytotoxicity and photocatalytic toxicity. Int J Mol Sci 21:1–49. https://doi.org/10.3390/ijms21176305
57. Rao TN, Riyazuddin BP et al (2019) Green synthesis and structural classification of Acacia nilotica mediated-silver doped titanium oxide (Ag/TiO2) spherical nanoparticles: assessment of its

antimicrobial and anticancer activity. Saudi J Biol Sci 26:1385–1391. https://doi.org/10.1016/j.sjbs.2019.09.005
58. Bhagat J, Ingole BS, Singh N (2016) Glutathione S-transferase, catalase, superoxide dismutase, glutathione peroxidase, and lipid peroxidation as biomarkers of oxidative stress in snails: a review. Invertebr Surviv J 13:336–349. https://doi.org/10.25431/1824-307X/isj.v13i1.336-349
59. Dayem AA, Hossain MK, Bin Lee S et al (2017) The role of reactive oxygen species (ROS) in the biological activities of metallic nanoparticles. Int J Mol Sci 18:1–21. https://doi.org/10.3390/ijms18010120
60. Jabłońska-Trypuć A, Wydro U, Wołejko E et al (2020) Possible protective effects of TA on the cancerous effect of mesotrione. Nutrients 12(5):1343. https://doi.org/10.3390/nu12051343
61. Zhao MX, Wen JL, Wang L et al (2019) Intracellular catalase activity instead of glutathione level dominates the resistance of cells to reactive oxygen species. Cell Stress Chaperones 24:609–619. https://doi.org/10.1007/s12192-019-00993-1
62. Chen H, Luo L, Fan S et al (2021) Zinc oxide nanoparticles synthesized from Aspergillus terreus induces oxidative stress-mediated apoptosis through modulating apoptotic proteins in human cervical cancer HeLa cells. J Pharm Pharmacol 73:221–232. https://doi.org/10.1093/jpp/rgaa043
63. Rahimi G, Mohammad KS, Zarei M et al (2022) Zinc oxide nanoparticles synthesized using Hyssopus officinalis L. extract induced oxidative stress and changes the expression of key genes involved in inflammatory and antioxidant Systems. Biol Res 55:1–10. https://doi.org/10.1186/s40659-022-00392-4
64. Yang D, Zhang M, Gan Y et al (2020) Involvement of oxidative stress in ZnO NPs-induced apoptosis and autophagy of mouse GC-1 spg cells. Ecotoxicol Environ Saf 202:110960. https://doi.org/10.1016/-j.ecoenv.2020.110960